Available on CMS information server

CMS NOTE-2008/008

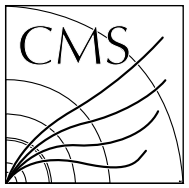

The Compact Muon Solenoid Experiment

CMS Note

Mailing address: CMS CERN, CH-1211 GENEVA 23, Switzerland

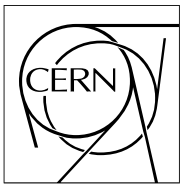

11 February 2008

A Study of Full Scale CMS Tracker Alignment using High Momentum Muons and Cosmics

G. Flucke, P. Schleper, G. Steinbrück, M. Stoye

Abstract

The positions of the silicon modules of the CMS tracker will be known to $O(100\ \mu\text{m})$ from survey measurements, mounting precision and the laser alignment system. However, in order to fully exploit the capabilities of the tracker, these positions need to be known to a precision of a few μm. Only a track-based alignment procedure can reach this required precision. Such an alignment procedure is a major challenge given that about 50000 geometry constants need to be measured. Making use of the novel χ^2 minimization program Millepede II an alignment strategy has been developed in which all detector components are aligned simultaneously and all correlations between their position parameters taken into account. Different datasets, such as Z^0 decays and cosmic muons, plus information about the mechanical structure of the tracker, and initial position uncertainties have been used as input for the alignment procedure. A proof of concept of this alignment strategy is demonstrated using simulated data.

1 CMS Tracker Alignment Challenge

A precise alignment of the silicon tracker of CMS [1, 2] is mandatory in order to fully exploit its physics capabilities. The tracker consists of 25644 silicon sensors which have altogether a surface of about 200 m^2. It is the largest silicon tracker ever built, having a diameter of 2.4 m and a length of 5.4 m. The silicon strip tracker is composed of several sub-detectors, namely the Tracker Inner Barrel (TIB), the Tracker Outer Barrel (TOB), the Tracker Inner Disks (TID), and the Tracker Endcaps (TEC). Some of the modules (stereo modules) are constructed using two individually read out silicon strip sensors, which are mounted with an angle of 100 milliradians with respect to each other in order to obtain two dimensional measurements. The pixel detector is divided into the Pixel Barrel (PB) and the Pixel Endcaps (PE). Figure 1 shows a schematic overview of one quarter of the tracker in the r-z projection and the pseudo-rapidity coverage. The sensor properties of pixel and strip tracker are listed in table 1. The modules of the TOB and the three outermost rings of the TEC hold two sensors, daisy chained; the two modules of each stereo pair are counted as a single unit for the alignment purpose, hence leading to 13300 modules altogether.

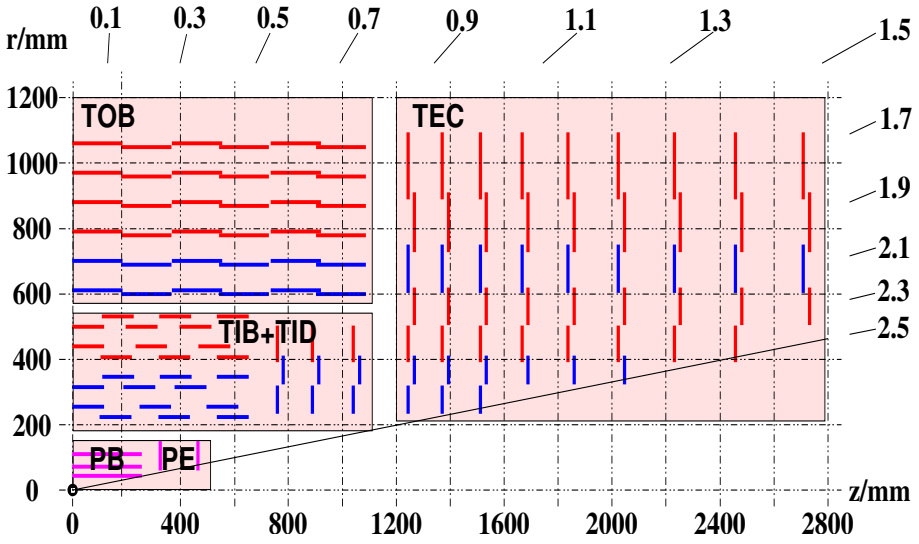

Figure 1: Layout of one quarter of silicon tracker in the r-z projection with η coverage indicated.

Table 1: Geometric properties and numbers of individually readout silicon detectors.

part	number	thickness [μm]	mean pitch [μm]
PB	768	285	100×150
PE	672	285	100×150
TIB	2724	320	80,120
TOB	5208	500	122,183
TID	816	320	81,119
TEC 1-4	2512	320	81-139
TEC 5-7	3888	500	126-172

The initial uncertainties on the module positions from the mounting precision, survey measurements, and the laser alignment system will be of the order of few hundred microns. The effect of such a misalignment on the performance is expected to be significant. For example, the transverse momentum resolution in the central region decreases from about 1 % to 5 % for muons with a transverse momentum of 100 GeV. Only track-based alignment procedures will be able to improve on this initial situation. To avoid significant adverse effects due to misalignment, the positions of detectors should be known to the order of a few μm, which is an order of magnitude smaller than the typical intrinsic resolution of the sensors. However, even small displacements can have an effect on track parameter measurements if the displacements are correlated.

The precision with which the tracker can be aligned is completely dependent on what datasets are available. This availability varies widely for different high energy physics experiments. Lepton colliders typically have a well

defined centre-of-mass energy, with the centre-of-mass frame and the experimental frame being identical (e.g. LEP experiments) or at least the transformation between the frames is well known (e.g. b-factories). Muon pair production in such an environment is an ideal source of tracks for alignment, as the muons are exactly back-to-back and have a *known momentum* value. Such events can be used as a *standard reference* to calibrate the momentum measurement via the alignment procedure. Hadron colliders do not have access to such a good reference sample, making detector alignment much more complicated.

In order to achieve a fast turn around, the CPU time for alignment should be of the order of hours and the memory required should not exceed few GBs.Assigning three alignment parameters to each single strip module and four parameters to the stereo modules and to the pixel modules, about 50000 alignment parameters are needed for the entire tracker. This is an order of magnitude larger than any previous alignment problem in high energy physics.

An alignment strategy is laid out in the next section, followed by an detailed description of the alignment algorithm (section 2). Using this algorithm χ^2-invariant deformations are identified and classified (section 3). In section 4 a full scale alignment study is shown, using muons of Z^0 decays and cosmic muons. The impact of different datasets and different options of the algorithm are also studied. Finally the effect of the remaining misalignment on the reconstruction quality is presented in section 5.

1.1 Alignment Strategy

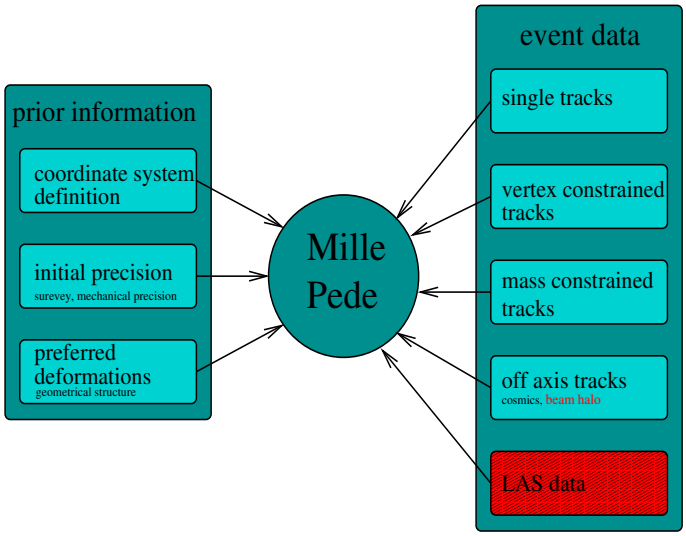

Figure 2: Schematic illustration of the alignment strategy. All elements of this strategy have been used in this study except the Laser Alignment System (LAS) and beam halo data which had not been available.

The aim of a track-based alignment procedure is to reduce the bias and uncertainty of the fitted track parameters and to minimize the χ^2 of the track fits by correcting the positions of the detector components. The minimization of the χ^2 is important to ensure track and vertex recognition, because the χ^2 of the track fit can be used to identify hits that make exceptionally large contributions to the χ^2 and hence are likely to be incorrectly associated to tracks. However, even with the χ^2 minimized and the pattern recognition working well, it is still possible to end up with biased measurements of track parameters due to misalignment. Correlated displacements of sensors that introduce a track parameter bias, but do not change the mean χ^2, are clearly a major challenge. Given this situation, a sophisticated alignment strategy will be required.

The most important ingredients for alignment are the datasets. In addition to tracks from pp collisions, beam halo and cosmic ray tracks will be important because they pass through detector components that are otherwise unconnected by tracks. In addition, correlated misalignment can be reduced with the help of reconstructed particle decays such as $Z^0 \to \mu\mu$. Datasets of interest are therefore:

- Tracks from pp collisions;
- Cosmic ray muon tracks and beam halo muons;
- Tracks from decaying particles, such as $Z^0 \to \mu\mu$;

- Laser alignment system tracks and survey measurements;

Another key ingredient are the known uncertainties on the sensor positions and the correlations between them, which are introduced by the mechanical support structures of the tracker. The information comes from:

- Mechanical mounting and survey precision;
- Support structure layout.

However, the use of this initial knowledge requires a good understanding of the temperature dependence of the mechanical properties, and the possible time evolution of the module positions. Generally, the information extracted in situ from event data is preferred. In addition to the datasets, certain symmetries of the track parameter distributions can be used to extract additional information about the sensor positions. Some examples of this are:

- Identical transverse momenta spectra for both muons in $Z^0 \rightarrow \mu^- \mu^+$ decays;
- Independence of the transverse momentum distributions on the azimuthal angle ϕ.

To make optimal use of these pieces of information, an alignment algorithm must be able to fulfill the following requirements:

- Inclusion of all correlations between position parameters;
- Incorporation of equality constraints between position parameters (e.g. via Lagrange Multipliers);
- Incorporation of survey measurements;
- Fast turn around time and computational feasibility;
- Special treatment of badly measured or incorrectly assigned hits (outliers);

The algorithm used in this study is briefly described in the next section. An overview of the alignment ingredients used is given in Figure 2.

1.2 Alignment Algorithms

Most track-based algorithms are based on the χ^2 minimization principle. At CMS a track typically consists of about 20 independent measurements such that the five parameters of a helix track are, in principle, overdetermined. These measurements, u_m, are compared to predictions from the track model. The predicted measurements, u_p, from the track model depend, for track j, on the vector of track parameters, $\boldsymbol{\tau}_j$, and the parameters, $\mathbf{p}$, that describe the position, orientation and deformation of the detectors. The normalized residual, z_{ij}, between the predicted hit position and the recorded measurement of hit i is given by:

$$z_{ij} = \frac{u_{ij;\,m} - u_{ij;\,p}(\boldsymbol{\tau}_j, \mathbf{p})}{\sigma_{ij}}. \tag{1}$$

The uncertainties, σ_{ij}, for each module do not contain correlations between the hit measurements, which are, in any case, generally not significantly correlated. Exceptions occur only if measurements from different sensors are combined into a single measurement (stereo modules) or if particle interactions with material are a major source of uncertainty, which is only the case for low momentum tracks.

Requiring optimal agreement between the track model and the data means minimizing a function that depends on the normalized residuals. Most commonly the function

$$\chi^2(\boldsymbol{\tau}, \mathbf{p}) = \sum_j \left(\sum_i z_{ij}^2(\boldsymbol{\tau}_j, \mathbf{p}) \right) \tag{2}$$

is minimized with respect to all $\boldsymbol{\tau}_j$ and $\mathbf{p}$. Generally, all overdetermined parameters from objects that are reconstructed in the tracker, like vertices for example, can be used for alignment.

2 Global Linear χ^2 Minimization with Constraints

2.1 Linearization of Normalized Residuals

The first step in the χ^2 minimization is to linearize the minimization problem. This is equivalent to a linearization of the normalized residuals z_{ij} in the χ^2-function:

$$\chi^2 = \sum_j \left(\sum_i z_{ij}^2(\boldsymbol{\tau}_j, \mathbf{p}) \right) \simeq \sum_j \left(\sum_i \frac{1}{\sigma_{ij}^2} \left(u_{ij;\,m} - u_{ij;\,p}(\boldsymbol{\tau}_{j0}, \mathbf{p_0}) + \frac{\partial u_{ij;\,p}}{\partial \mathbf{p}} \mathbf{a} + \frac{\partial u_{ij;\,p}}{\partial \boldsymbol{\tau}_j} \delta\boldsymbol{\tau}_j \right)^2 \right), \quad (3)$$

where $\mathbf{p_0}$ are the initially-assumed geometry parameters and $\boldsymbol{\tau}_{j0}$ are the initially-assumed track parameters. The geometric correction parameters $\mathbf{a} = \delta\mathbf{p}$ are referred to as alignment parameters in the following. The alignment parameters are known as global parameters, as they are not specific to a single track or event. The parameter corrections for a track (or other reconstructed objects like a vertex) are specific to a single event and hence the parameters $\delta\boldsymbol{\tau}_j$ are known as local parameters. The linearized minimization leads to a system of linear equations that needs to be solved [5]. The number of free parameters in these equations is given by the total number of local and global parameters. The number of local parameters can be of the order of millions. In addition, there are some 50000 global parameters. This leads to an symmetric square matrix with millions of rows.

2.2 Matrix Reduction

Given the size of the matrix involved, its reduction is mandatory. A customized algorithm that makes use of the special nature of local parameters is able to fulfill this task. In case of track-based alignment individual tracks are independent of each other apart from the fact that they use a common geometry description of the tracker. This leads to a special structure of the (normal equation) matrix:

$$\left(\begin{array}{c|c|c|c} \sum \mathbf{C}_j & \dots & \mathbf{G}_j & \dots \\ \hline \vdots & \ddots & 0 & 0 \\ \hline \mathbf{G}_j^T & 0 & \boldsymbol{\Gamma}_j & 0 \\ \hline \vdots & 0 & 0 & \ddots \end{array}\right) \left(\begin{array}{c} \mathbf{a} \\ \hline \vdots \\ \hline \delta\boldsymbol{\tau}_j \\ \hline \vdots \end{array}\right) = \left(\begin{array}{c} \sum \mathbf{b}_j \\ \hline \vdots \\ \hline \boldsymbol{\beta}_j \\ \hline \vdots \end{array}\right), \quad (4)$$

where the elements are given by:

$$(\boldsymbol{\Gamma}_j)_{kl} = \sum_i \frac{\partial z_{ij}}{\partial \tau_{jk}} \frac{\partial z_{ij}}{\partial \tau_{jl}}\,,\ (\boldsymbol{\beta}_j)_k = \sum_i \frac{\partial z_{ij}}{\partial \tau_{jk}} z_{ij}\,,\ (\mathbf{C}_j)_{kl} = \sum_i \frac{\partial z_{ij}}{\partial a_{jk}} \frac{\partial z_{ij}}{\partial a_{jl}}\,,$$

$$(\mathbf{b}_j)_k = \sum_i \frac{\partial z_{ij}}{\partial a_{jk}} z_{ij}\,, \text{and } (\mathbf{G}_j)_{kl} = \sum_i \frac{\partial z_{ij}}{\partial a_{jk}} \frac{\partial z_{ij}}{\partial \tau_{jl}}$$

This structure can be exploited to reduce the matrix size. The sub-matrices $\boldsymbol{\Gamma}_j$ include only derivatives with respect to local parameters, while the sub-matrices $\mathbf{C}_j$ depend only on global parameters. The matrices $\mathbf{G}_j$ include both. Products of global derivatives and the normalized residuals appear in $\mathbf{b}$, and $\boldsymbol{\beta}_j$ consist of local derivatives and the normalized residuals. A matrix $\mathbf{C}'$ and a vector $\mathbf{b}'$ can be defined as follows:

$$\mathbf{C}' = \sum_j \mathbf{C}_j - \sum_j \mathbf{G}_j \boldsymbol{\Gamma}_j^{-1} \mathbf{G}_j^T \qquad \mathbf{b}' = \sum_j \mathbf{b}_j - \sum_j \mathbf{G}_j (\boldsymbol{\Gamma}_j^{-1} \boldsymbol{\beta}_j) \quad (5)$$

This leads to a much smaller equation system, which only contains the global parameters, $\mathbf{a}$:

$$\left(\begin{array}{c} \mathbf{C}' \end{array}\right) \left(\begin{array}{c} \mathbf{a} \end{array}\right) = \left(\begin{array}{c} \mathbf{b}' \end{array}\right) \quad (6)$$

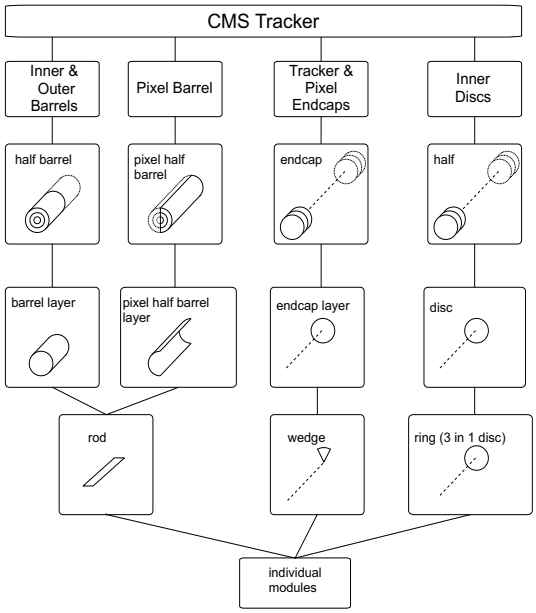

Figure 3: Illustration of the hierarchical support structures used for the alignment study. This software implementation of the support structures follows the physical support structures. However, small differences to the hardware structures do exist, e.g. the physical outer barrels do not have layers as support structures.

Using this matrix size reduction from several million parameters to only the number of global parameters without losing correlation and precision is the core idea behind the Millepede algorithm [3]. In the course of the matrix reduction, correction parameters, $\delta\boldsymbol{\tau}_j$, for each track and for a given geometry are calculated:

$$\delta\boldsymbol{\tau}_j = \mathbf{\Gamma}_j^{-1}\beta_j \tag{7}$$

This is essential in order to extract the χ^2 of the track fits for a given geometry.

2.3 Constraints

A set of linear equality constraints on the alignment parameters can be expressed by a matrix equation: $\mathbf{Aa} - \mathbf{m} = 0$. These constraints are applied via Lagrange Multipliers leading to the following matrix equation [5]:

$$\left(\begin{array}{c|c} \mathbf{C}' & \mathbf{A}^T \\ \hline \mathbf{A} & 0 \end{array}\right)\left(\begin{array}{c} \mathbf{a} \\ \hline \lambda \end{array}\right) = \left(\begin{array}{c} \mathbf{b}' \\ \hline \mathbf{m} \end{array}\right) \tag{8}$$

If Lagrange Multipliers are used the matrix is no longer positive definite, which has to be kept in mind when choosing methods to solve the equation system.

2.3.1 Support Structure Constraints

The CMS Tracker consists of a hierarchy of support structures as illustrated in Figure 3. Each support structure can be given additional alignment parameters. If structures at different levels of the hierarchy are aligned at the same time, equality constraints need to be applied in order to avoid a singular matrix. For example, a translation of a support structure corresponds directly to translations of all its subcomponents. A common translation of the subcomponents could cancel this movement, so common translations of the subcomponents with respect to support the structure must be forbidden by applying equality constraints. The calculation of the derivatives of the rigid body alignment parameters of support structures and the calculation of the equality constraints can be found in [6].

Table 2: Memory requirements for the matrix $\mathbf{C}'$: n is number of global parameters, m the band width for the Choleskey band method and q the matrix density. The space needed for equality constraints is not included.

methods	memory space required [8 byte words]
inversion	n+n(n-1)/2
diagonalization	n+n(n-1)/2+n^2
band Cholesky	nm
GMRES (sparse)	n+qn(n-1)3/4

2.4 χ^2-penalties

χ^2-penalties are initial uncertainties σ_p (presigmas) given to individual alignment parameters. For each alignment parameter, a term $1/\sigma_p^2$ is added to the diagonal matrix entry of the parameter. The χ^2-penalties are therefore defined with respect to the alignment parameters of the previous iteration within Millepede. This means that alignment corrections that are significantly larger than the corresponding presigma are allowed after several iterations. Iterations are needed for outlier rejection in any case. Assigning presigmas does improve the stability of the solution (condition) of the matrix equation, thereby avoiding numerical problems. Optimal values of the presigmas of the alignment parameters of the modules were found to be a factor of ten smaller than the initial position uncertainties with respect to the next supporting structure [6]. The presigmas of support structures were set to their position uncertainties.

2.5 Linear Equation Solvers

The number of elements in the matrix $\mathbf{C}'$ in equation 6 is equal to the number of alignment parameters squared. In the case of the CMS tracker, there are about 50000 parameters, making a matrix inversion not feasible with the currently available computing power. However, there are algorithms that can solve linear equations much faster than by inversion, especially if the matrix is sparse (contains many zero elements). These algorithms do not modify the matrix whilst solving it. They require only the products of the matrix with vectors, which can be very fast for a sparse matrix. Several methods are implemented in Millepede II.

Inversion: The CPU time needed for inverting a $n \times n$ matrix scales with n^3 and the memory needed to store the matrix scales with n^2. The inverted matrix is also the covariance matrix.

Diagonalization: Even more computing power is needed in order to diagonalize the matrix. However the eigenvectors and eigenvalues that are determined can be physically interpreted. Eigenvectors with small eigenvalues have little impact on the overall χ^2 and are therefore not well determined.

GMRES: If the matrix $\mathbf{C}'$ is sparse the memory demand can be reduced by storing only non-zero elements.The memory requirements are compared to other methods in table 2. If only tracks from the interaction point are used, the density (fraction of non zero elements), q, of the matrix is about 1%. Cosmic muons however also cross detector regions which are not connected by a single tracks from the interaction point, leading to a denser matrix. If tracks are refitted with a common vertex, and cosmic muons and beam halo muons are used, the matrix density easily exceeds 10%.
Millepede II incorporates the GMRES method [7]. It is a more generic version of the MINRES algorithm [8], which in contrast to GMRES, can only be applied to positive definite matrices. Here the speed of convergence is improved by multiplying the matrix equation by an approximate solution (see below) of the inverse matrix, a procedure known as preconditioning.

Variable-Band Cholesky: Cholesky decomposition [9] can be used to solve a system of linear equations that can be represented by a symmetric matrix. If the matrix is a symmetric band matrix, this method is very fast. Only the matrix elements within the band need to be stored which requires only little memory. However, the matrix that is built in the course of the χ^2 minimization is not a band matrix. Ignoring the elements outside the chosen band means ignoring some correlations between alignment parameters. Hence, the solution obtained via the band Cholesky is an approximate solution. The variability of the band size allows the inclusion of equality constraints.

Table 3: Influence function and weight factor function derived from different outlier rejection functions and the χ^2 function.

function $f(z)$	influence(z)=$\frac{df}{dz}$	weight factor(z)=$\frac{df}{dz}\frac{1}{z}$
$\chi^2 \rightarrow \frac{z^2}{2}$	z	1
Huber $\rightarrow \begin{cases} \frac{z^2}{2} & \text{if}\lvert z\rvert < \mathrm{C_H} \\ C_H(\lvert z\rvert - \frac{C_H}{2}) & \text{if}\lvert z\rvert > \mathrm{C_H} \end{cases}$	z C_H	1 $\frac{C_H}{\lvert z\rvert}$
Cauchy $\rightarrow \frac{C_C^2}{2}\ln(1+(\frac{z}{C_C})^2)$	$z/(1+(\frac{z}{C_C})^2)$	$1/(1+(\frac{z}{C_C})^2)$

The constraints are implemented via the matrix $\mathbf{A}$ as shown in equation 8. The variable bandwidth is set such that the full matrix $\mathbf{A}$ is included. The variable-band Cholesky method is used for preconditioning of the GMRES method.

2.6 Outlier Rejection

In the χ^2-minimization procedure, the influence of a normalized residual increases linearly with its absolute value. Recorded hits that are many standard deviations away from the expected hit position (outliers) therefore have a large impact on the result. The minimization of the χ^2-function is only optimal if the uncertainties are Gaussian. Due to misassigned hits or non-Gaussian hit reconstruction errors, this assumption is not valid. For outlier rejection mechanism, iterations will be required in order to achieve optimal performance. In Millepede, two outlier rejection methods have been developed. The first one is a track rejection while in the second hits are down-weighed.
In the former, when performing the matrix reduction within Millipede, the χ^2 and the number of degrees of freedom (ndof) for the track fit in each iteration are determined (equation 7). A cut on the χ^2/ndof is applied to reject badly reconstructed tracks. However, in the first iteration the χ^2 is generally large, since the sensors are misaligned and therefore only loose cuts can be applied. The cuts are then tightened with each iteration, since the χ^2 decreases with the improved alignment precision. However, the χ^2/ndof values of corrupted tracks remain large; hence they are rejected.
In the other outlier rejection mechanism, the impact of outlier hits is reduced by down-weighting their influence in the minimization procedure. A standard method (M-estimates) is not to minimize the χ^2-function but a different function F of the normalized residuals:

$$F(\boldsymbol{\tau}, \mathbf{a}) = \sum_j \Big(\sum_i f(z_{ij}(\boldsymbol{\tau}_\mathbf{j}, \mathbf{a})) \Big)$$

where f can be the Huber function or the Cauchy function (see table 3). If the Huber function is used the influence of normalized residuals that are larger than a parameter C_H, remains constant. A standard value for C_H is 1.345, which would result in an increase of the alignment uncertainty of 5%, if the error distributions are Gaussian. If the Cauchy function is used the influence decreases even for very large normalized residuals. The influence $\frac{df}{dz}$ and weight $\frac{df}{dz}\frac{1}{z}$ of a hit in the fit procedure for these functions are shown in Figures 4 and 5, respectively.
The track fit (equation 7) is done 5 times when using the down-weighting method, since the new weights lead also to new track parameters. For the first two iterations the Huber-function is used, afterwards the Cauchy-function. A small average weight of the hits from a track indicates that a number of hits are incorrectly measured. Hence, it is reasonable to reject these tracks.

2.7 Computational Layout

An important aspect of alignment is the time needed for the analysis. It is therefore important that the information used by Millepede is collected in an efficient way. Collecting the necessary derivatives and measurements from the data can be parallelized. Therefore Millepede II is split into two parts, one part (Mille) produces binary files of the data needed for the alignment procedure. This part was interfaced to the CMS software. The other part (Pede) determines the alignment parameter from the binary files and is a standalone FORTRAN program. The separation between the CMS software and Pede makes it possible to use Pede easily in other experiments as well. The output of Pede are the alignment parameters used later on for reprocessing.

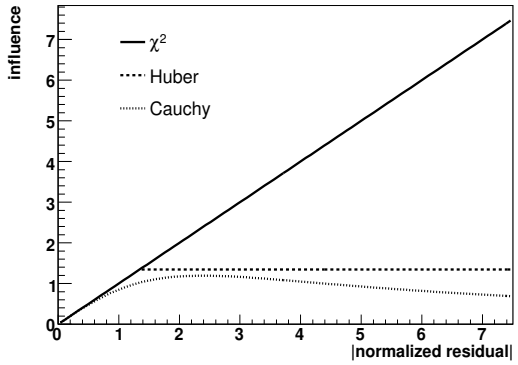

Figure 4: Influence functions for χ^2, Huber, and Cauchy methods.

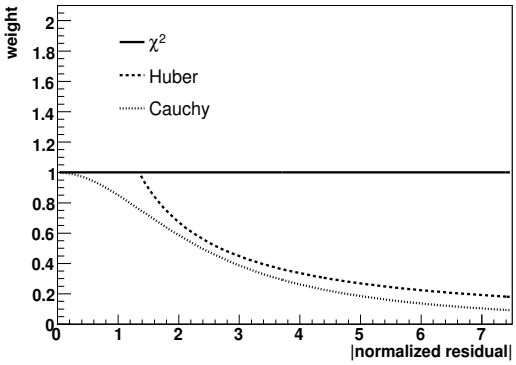

Figure 5: Weight factor functions for χ^2, Huber, and Cauchy methods.

3 χ^2 Invariant Deformations

The diagonalization method of Millepede II has been used to identify the χ^2 invariant deformations described in section 1.1. The final alignment parameters $\mathbf{a}$ in terms of the normalized eigenvectors , $\mathbf{e}_k$, are given by:

$$\sum_k \alpha_k \mathbf{e}_k = \mathbf{a}. \tag{9}$$

The eigenvectors with the smallest eigenvalues are the least well determined, since the eigenvalue is given by $1/\sqrt{\sigma_k}$, where σ_k is the uncertainty on the amplitude α_k of the eigenvector $\mathbf{e}_k$. The deformations corresponding to eigenvectors with the smallest eigenvalues were applied to the geometry in order to visualize the deformations. The diagonalization method is CPU intensive and hence the number of alignment parameters is limited to $O(10000)$. The alignment parameters and the dataset used to identify these deformations are described below.

Alignment Parameters: In order to limit the computing requirements to an acceptable level, the smallest support structures, rather than the individual modules, were used in the barrel region for the study of deformations. These are the strings, rods (for the TIB and TOB) and ladders (for the PB) consisting of 3, 6, or 8 individual modules along the z (beam) direction, respectively. The alignment parameters per string, rod or ladder are the three translations u, v, w and the rotation, γ, around the normal of the support structure, all of which are illustrated in Figure 6. For structures that consist only of single-sided strip modules, the insensitive direction along the strips (v) is neglected. The parameters are summarized in table 4.

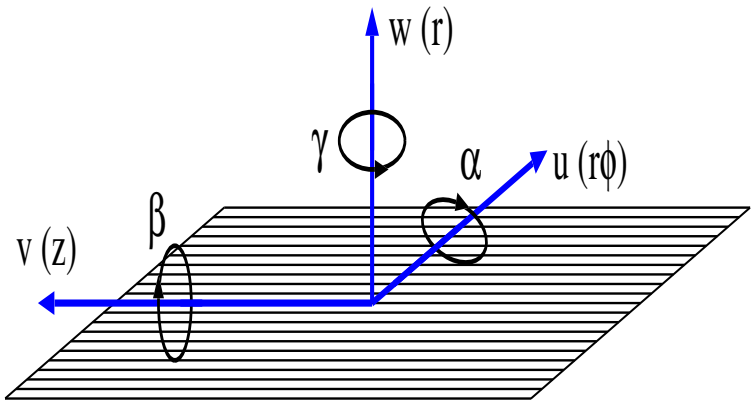

Figure 6: Schematic illustration of the alignment parameters. In brackets $(r, z, r\phi)$ are corresponding directions in the global CMS coordinate system in case of barrel modules.

Table 4: Alignment parameters used for strings, rods and ladders in the study of χ^2 invariant deformations.

type	number	alignment parameters	corresponding global coordinates
rods/strings	1340	u, v (if stereo), w, γ	$r\phi$, z (if stereo), r, rot$_r$
ladders	90	u, v, w, γ	$r\phi$, z, r, rot$_r$

Dataset and Selection: The $Z^0 \rightarrow \mu\mu$ decay is often called the "golden channel" for alignment. The high momentum of the muons and the relatively large muon mass lead to very small amounts of multiple scattering. In addition, pattern recognition and particle identification are relatively straight-forward for these isolated high momentum muons. The dataset used contains one million Drell-Yan $Z^0/\gamma^* \rightarrow \mu\mu$ events produced with a pileup expected for nominal luminosity. The invariant mass of the muon pair is required to be at least 80 GeV. Each track is required to have at least 8 measurements within the barrel region and a transverse momentum of more than 15 GeV. All measurements from detectors which are not included in this down-sized alignment study (endcap modules) are ignored.

Results: A set of basic χ^2-invariant deformations has been identified by their small eigenvalues. An example of the visualization of a badly-determined eigenvector deformation is shown in Figures 7 and 8. They show an oscillation of the displacements in the radial direction r and in the tangential direction $r\phi$ as a function of the azimuthal angle ϕ. Functions of the form:

$$\Delta r(\phi) \sim \cos(n\phi + \omega) \quad \Delta r\phi(\phi) \sim \sin(n\phi + \omega) \quad \Delta z(\phi) \sim \cos(n\phi + \omega) \tag{10}$$

were fitted to the data in Figure 8. Here ω is a constant shift and n is an integer mode number. Each mode n occurs twice, once with a constant shift $\omega = \omega_0$ and once with a shift $\omega = \omega_0 + 90°/n$.
Mode 0 would be equivalent to a tracker expansion. This was the only mode found to impact the χ^2 value significantly, since the overall scale is fixed by the well known strip-pitch distances. Generally an expansion in r between different layers is accompanied by compression in $r\phi$ within these layers in order to keep the χ^2 of track fits small [6].

Another category of basic χ^2-invariant deformations are bending and shearing. Their average displacement in the r-ϕ direction can be described as a function of the radius of the modules:

$$\langle \Delta r\phi \rangle(r) \simeq p_0 + p_1 r + p_2 r^2 \quad \langle \Delta z \rangle(r) = z_0 + z_1 r \tag{11}$$

If the parameter p_2 is non zero, this is especially worrying, since it directly effects the curvature measurement. The fit, shown in Figure 9, of the equation 11 to the data clearly illustrates that this function approximates well the χ^2-invariant deformation. The bending and shearing deformation can vary along the z-axis, leading to a twist of the tracker. Also this deformation was among those described by the eigenvectors with the ten smallest eigenvalues. A summary of the basic deformations which were observed is illustrated in Figure 10. The observed deformations are likely to remain after the alignment procedures and it is therefore important to understand their effect and find means to reduce their impact. More detailed studies on the deformations can be found in [6]. The use of datasets like cosmic muons and constraints like the vertex constraint for particles from the same interaction point are essential to fulfill this task, as will be seen in the following sections.

4 Full Tracker Alignment Case Studies

In this section alignment studies using all strip and pixel modules in both barrel and endcap are presented.

The *first data* scenario, as described in [10], is used as initial misalignment. This misalignment scenario is the one that is meant represent approximately the initial position uncertainties at startup. The correlated nature of displacements due to common support structures of modules is taken into account. The pixel modules are assumed to be aligned to about 15 μm in this scenario. The initial position uncertainties are shown in table 5.

The full tracker is aligned, all of the pixel and strip detector of barrel and endcaps.The module alignment parameters are defined with respect to center of the half barrels or the endcaps, respectively. The initial position uncertainty of rods is similar to the module position uncertainty and since rods only consist of a small number of sensors this level was skipped. The layer levels are also skipped. The layers do not exist as support structure in the outer barrel

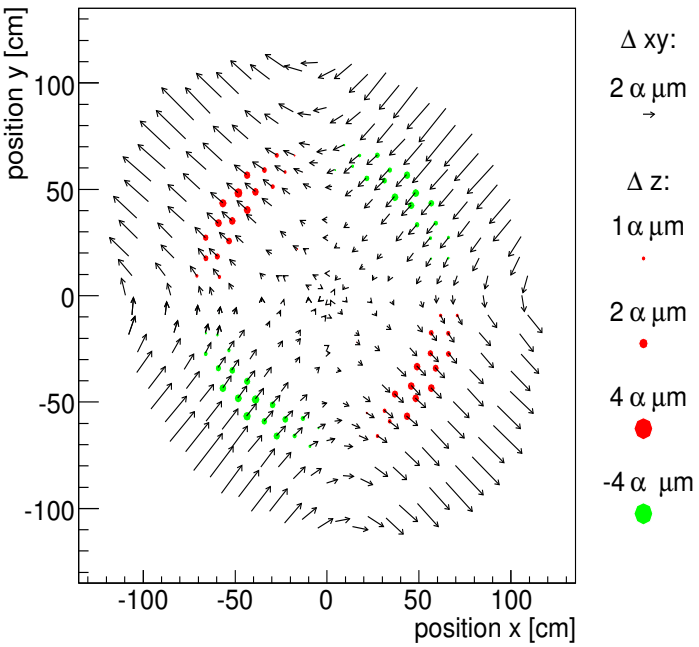

Figure 7: Illustration of the eigenvector of r-$r\phi$ mode 2 (see text). The radii of the circles represent the displacements in the z coordinate for the 2D detectors only. The colors decode the sign of the z displacements. The arrows indicate the displacements in the $r\phi$-plane. The amplitude α is the badly-determined parameter (equation 9).

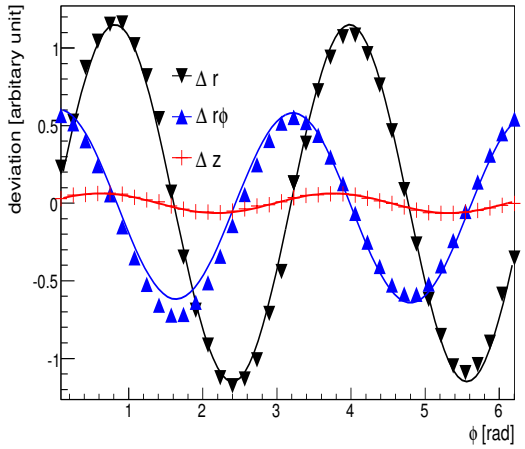

Figure 8: Displacements in $r, r\phi$, and z of rod positions in the fifth layer as a function of ϕ. The displacements correspond to a χ^2-invariant eigenvector. An r-$r\phi$ oscillation of mode 2 (equation 10) is fitted to the displacements.

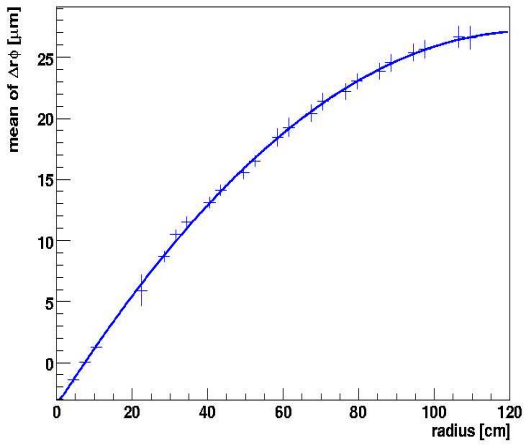

Figure 9: Fit of bending deformation function (equation 11) to a χ^2-invariant deformation.

a) sheering (red) and bending (green) in rϕ:

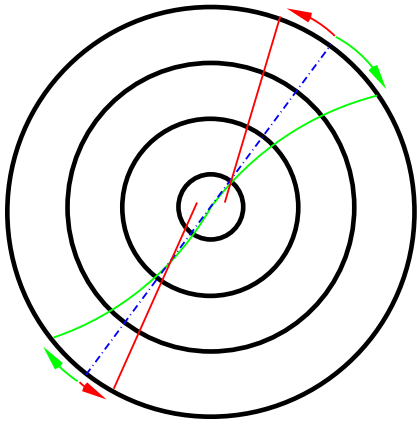

b) sheering in z:

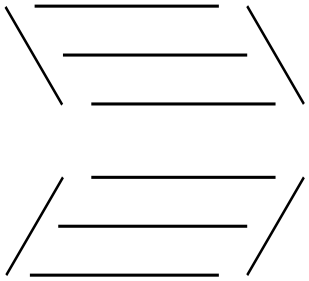

c) r-rϕ mode 1 (or sheering in x):

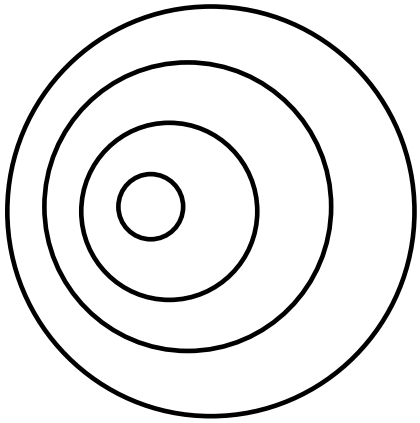

d) r-rϕ mode 2:

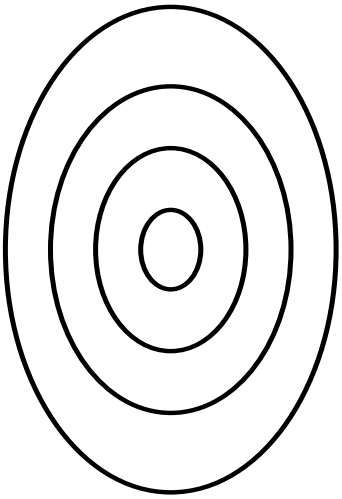

e) twist of barrel:

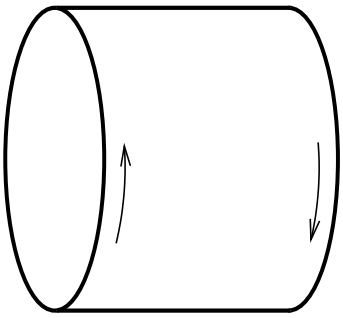

Figure 10: Schematic illustration of the χ^2 invariant deformations.

and are also generally not misaligned in the *first data* scenario. Each object is given four alignment parameters: the translation parameters u, v, w, and the rotation parameter γ. The parameter v is skipped for single-sided strip modules. Altogether this amounts to 44432 alignment parameters.
The innermost 24 sensors of each pixel endcap are not aligned since no track, which passes the selection criteria, passed them. The Z^0 sample described in the previous section is used. Half a million events are used with a vertex constraint, forcing the two muon tracks to a common vertex. In addition the Z^0 mass and width (approximated by a Gaussian) is used as input to the fit. A detailed description of this procedure can be found in [12]. Single muons, without any vertex or mass constraints, from 1.5 million Z^0 events were used to mimic 3 million $W\rightarrow \mu\nu$ events. These data roughly correspond to an integrated luminosity of 0.5 fb^{-1} of data taking. In addition a dataset of 25000 simulated cosmic ray muons with a momentum of at least 50 GeV was used. All the cosmic ray muons transverse the central barrel region. The pattern recognition was assumed to work perfectly for tracks from cosmic muons, in order to avoid additional uncertainties from a pattern recognition that has not yet been fully developed. Details of the simulation of cosmic muons can be found in [6]. All cosmic ray tracks were required to consist of at least 18 measurements and have an initial χ^2/ndof value below 10.

The applied presigmas for the alignment parameters of the modules are chosen to be a factor of 10 smaller than the initial uncertainties in the misalignment scenario. The presigmas for parameters of higher level structures are set to exactly equal the misalignment uncertainties. The applied presigmas are summarized in table 5.

The coordinate system is defined by the constraint that the sum of the alignment parameter vectors of the pixel half barrels has to be zero. Hence the average position of the pixel modules defines the origin of the coordinate system. In order to solve such a large alignment problem, the GMRES (see section 2) method in Millepede II is used. The linear equation system is preconditioned using the result of the band Cholesky method with a bandwidth of 6. Outlier hit down-weighting is used and tracks with an average weight of hits below 80% are rejected. The refit of tracks (local fit) is done with 5 iterations, since outlier down-weighting is applied. The number of the iterations for alignment parameter iterations (global fit) is also set to 5.

4.1 Alignment Results

The alignment results are presented for the *first data* misalignment scenario, which was used as the starting point for the alignment procedure. The results are compared to the *long term* scenario. The *long term* misalignment scenario was an estimate used in the CMS Physics Technical Design Report (PTDR) [11], of the achievable alignment precision after reaching about 1 fb^{-1} of integrated luminosity. However, the results of the study do not include uncertainties from systematic effects like uncertainties on the magnetic field for e.g..
Figure 11 shows the remaining displacements after alignment for the barrel and endcap modules. The calculated positions in the best measured direction (rϕ) for the barrel (strip and pixel) modules have an uncertainty of only about 10 μm. For the endcap (strip and pixel) modules, the mean of the position residuals in rϕ after the alignment

Table 5: Initial uncertainties according to the *first data* scenario [10], as used for the alignment procedure. A * denotes uncertainties that are assumed for alignment, but are zero in the simulation of the *first data* misalignment scenario. The presigmas applied for larger support structures are identical the their initial uncertainty, while the presigmas of the modules († rows) are a factor of ten smaller than their initial uncertainties. Note that rods, ladders, and petals have been misaligned, but are not introduced as alignment objects in this study.

type	Δ u [μm]	Δ v [μm]	Δ w [μm]	$\Delta\ \gamma$ [μrad]
PB half barrels	10	10	10	10
TIB half barrels	105	105	500	90
TOB half barrels	67	67	500	59
PE endcap	5	5	5	5
TID layers	400	400	400	100
TEC endcap	57	57	500	46
TPB modules†	13	13	13	10*
TIB modules†	200	200	200	10*
TOB modules†	100	100	100	10*
TPE modules†	2.5	2.5	2.5	10*
TID modules†	105	105	105	10*
TEC modules†	20	20	20	10*

procedure is around 5 μm and with a spread of 23 μm.
For the pixel modules the difference between true and estimated positions is presented in Figure 12. The remaining position uncertainty in rϕ for the pixel barrel modules of 1 μm after alignment is an order of magnitude smaller than the *long term* estimate. The pixel sensor position uncertainties are of the order of a few μm for all directions and module types. The barrel module positions are generally better determined than those of the endcap modules.
The residuals between the true and estimated position in rϕ have been studied separately for the different detector components TIB, TID, TOB, and TEC (Figure 13). Note that the double peak structure for the TOB modules is explained in the following paragraph. The position estimates improve with decreasing distance of the modules from the pixel detector. The intrinsic resolution of the modules closer to the beam line is generally better by construction and the number of hits larger. Furthermore, the displacements due to global deformation increase with distance from the pixel detector, whose sensors define the origin of the coordinate system.
The overall remaining misalignment is dominated by a global χ^2 invariant deformation, that is, an r-$r\phi$ oscillation of mode one, with the maximum of r displacement at ϕ close to 90° (Figure 14). A typical cosmic muon trajectory, which crosses the detector close to vertical, is also shown. It can be seen that the deformation displaces the modules in a direction almost parallel to a typical cosmic track, hence the hit measurements on the sensors are not strongly influenced by this deformation. Figure 15 shows a similar oscillation with its maximal amplitude in a different direction. In this case a typical cosmic track would be kinked and hence the this mode is suppressed by the use of cosmic muons. The studies performed here have shown that this is indeed the case.
The remaining oscillation is clearly visible in the displacements in $r\phi$-direction of the last layer of the barrel modules (Figure 16). Figure 17 shows the average displacements in y as a function of the radius of the module position. A linear function $\langle \Delta y \rangle (r)$ would be expected for the displacement illustrated in Figure 14 and, as can be seen in Figure 16, this is indeed the case. This oscillation also explains the double peak like structure in the residual distribution for the outer barrel modules (Figure 13, b). The peak at about 15 μm is caused by modules with a ϕ position around 0, while the peak at -15 μm is due to the modules with a ϕ position around $\pm\pi$.

Computing Requirements The datasets in this study give a matrix density of 8.6% which translates to less than 2 GB of memory. The CPU time used on a 64 Bit CPU is 1.2 hours.
When low energy cosmic rays are included, the alignment result does not significantly improve but the additional data lead to a higher matrix density (15%) because of the larger variation in the direction of flight. The CPU time needed in this case increases to two hours. The building of the matrix takes about 50 minutes, whilst the solving of the matrix equation takes about 10 minutes, but is done five times in the course of the outlier rejection procedure.
It can therefore be concluded that the computing requirements are reasonable and can accommodate additional alignment parameters and datasets without problem.

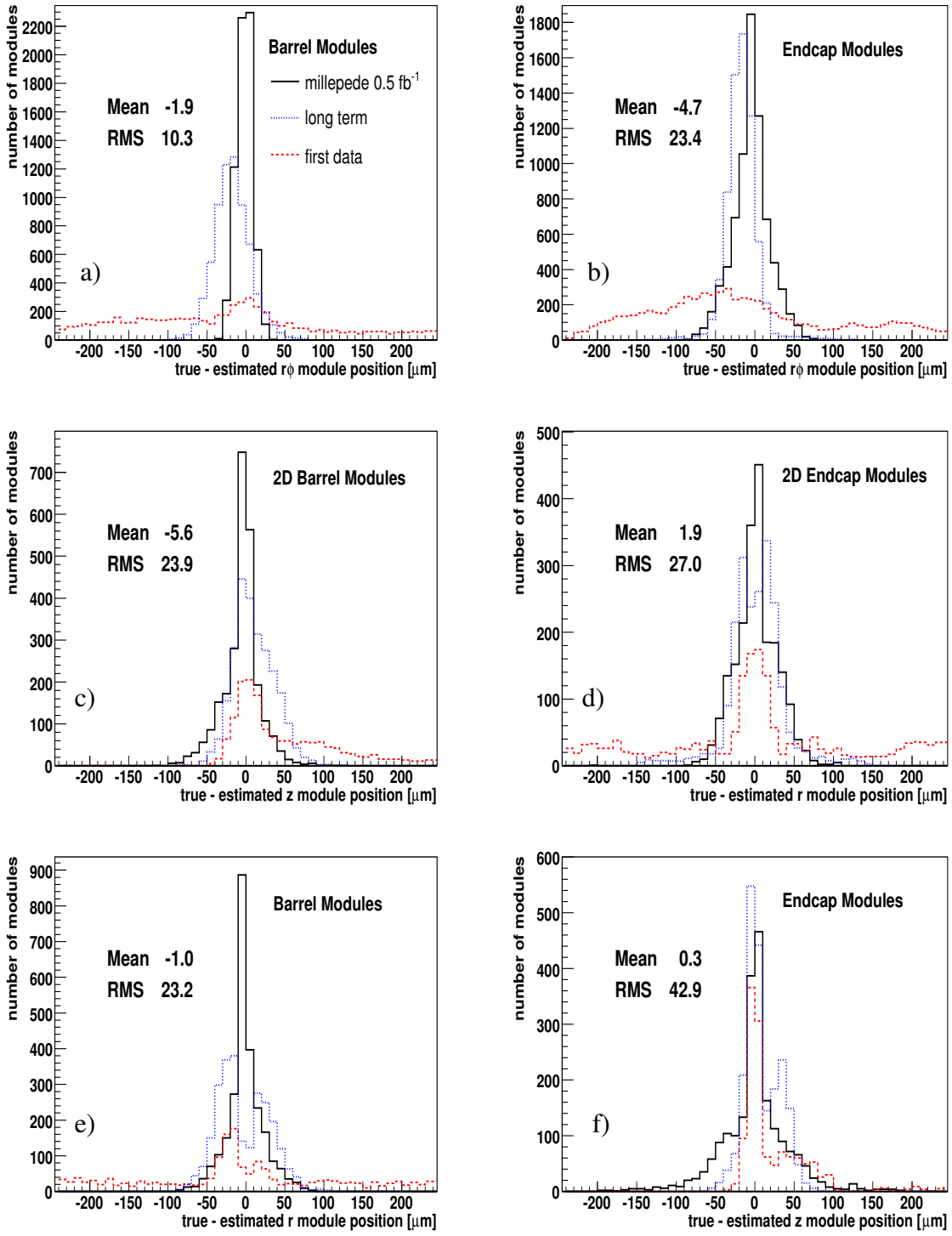

Figure 11: Residuals between true and estimated module positions in different directions and separately for barrel (left) and endcap (right) modules for the *first data* scenario, the *long term* scenario, and the result of the alignment procedure. The first row (a,b) shows the displacements in the $r\phi$ coordinate, the second row (c,d) the displacements in the other measured direction for stereo modules, and the third row the displacements in the direction normal to the sensor surface.

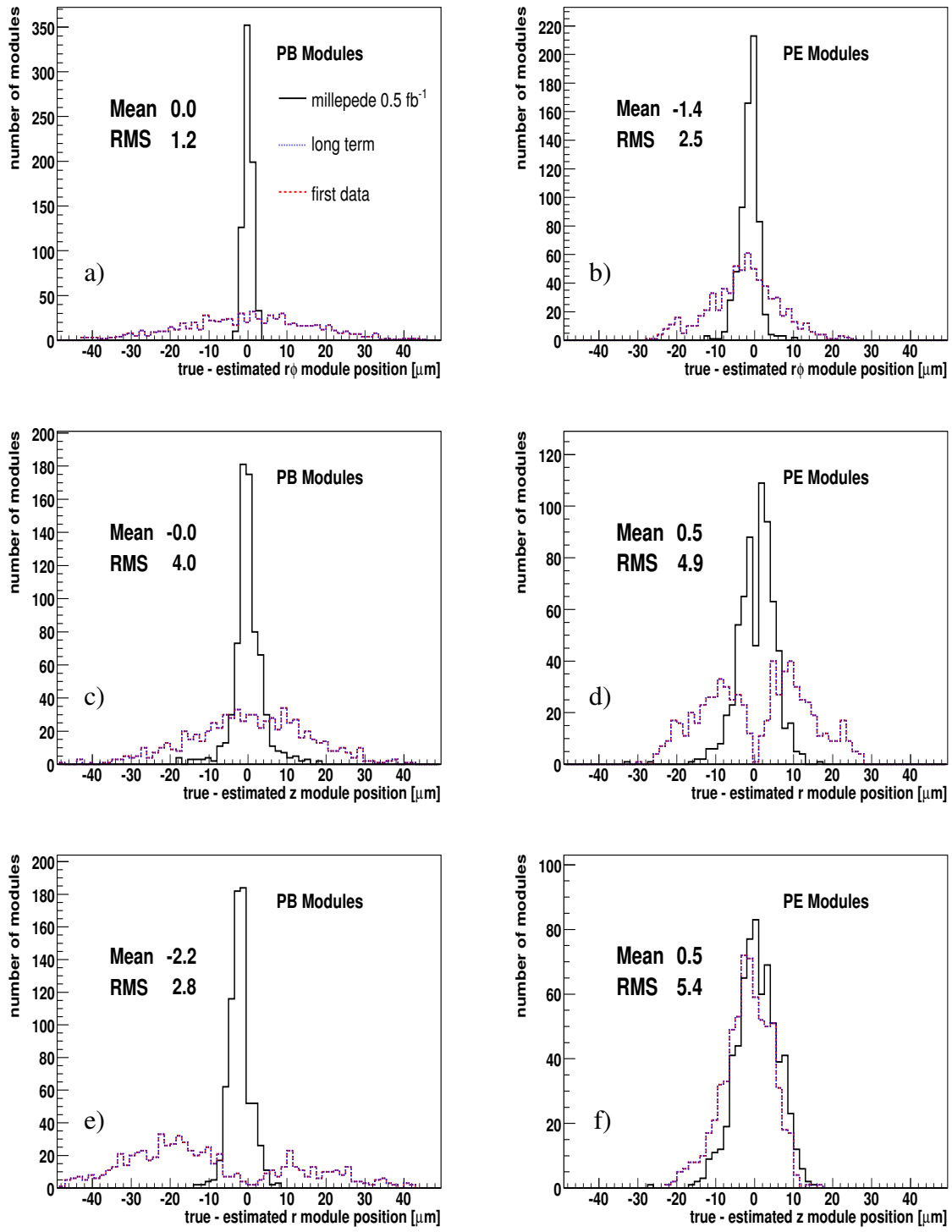

Figure 12: Residuals between true and estimated module positions in different directions and separately for pixel barrel (left) and pixel endcap (right) modules for the *first data* scenario, the *long term* scenario, and after the alignment procedure. The misalignment of the pixel modules are the same for the *long term* and the *first data* scenarios, which is a feature of the scenarios. The first row (a,b) shows the displacements in the rϕ direction, the second row (c,d) the displacements in the other measured direction, and the third row the displacements in the r (barrel) and z (endcap) coordinate directions.

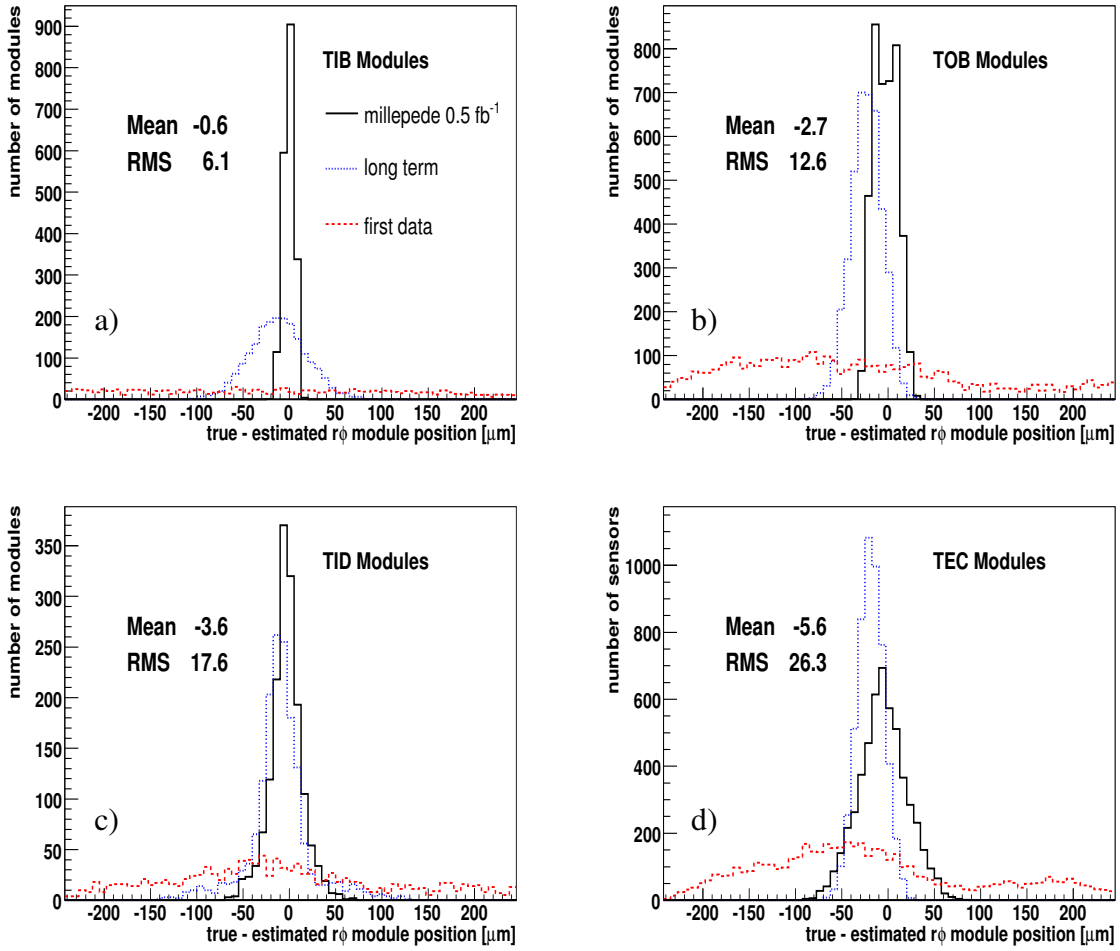

Figure 13: Residuals between true and estimated module rϕ positions for different detector components from the *first data* scenario, the *long term* scenario, and after the alignment procedure.

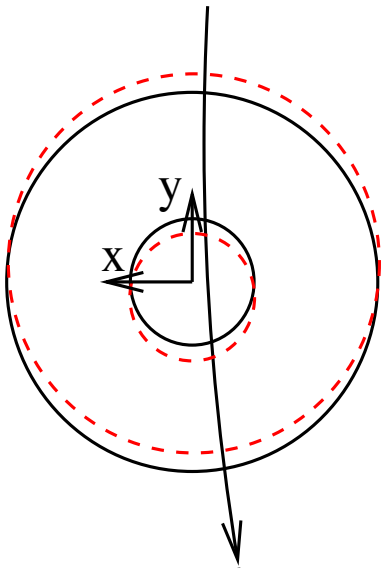

Figure 14: r-rϕ mode with a maximum amplitude of the r oscillation in the direction of y. The dashed lines illustrated the displaced geometry. In addition a typical cosmic trajectory is illustrated.

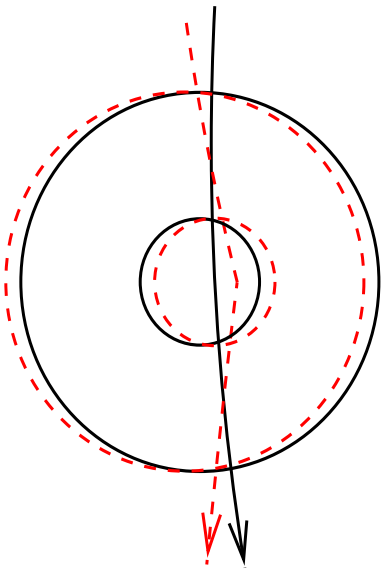

Figure 15: r-rϕ mode with a maximum amplitude of the r oscillation in the direction of x. The dashed lines illustrated the displaced geometry. In addition a typical cosmic trajectory is illustrated. The dashed trajectory illustrates the effect of the misalignment on the reconstructed track.

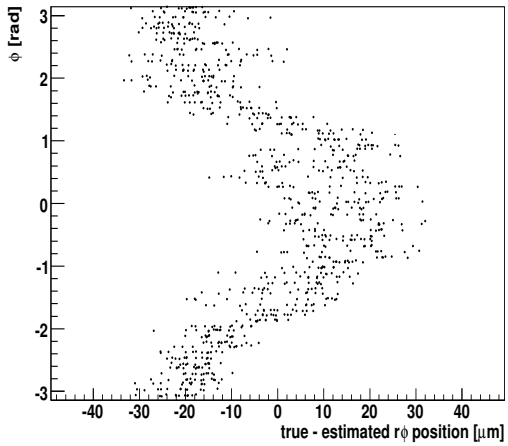

Figure 16: The displacements in rϕ of the barrel modules of the last layer versus ϕ after alignment.

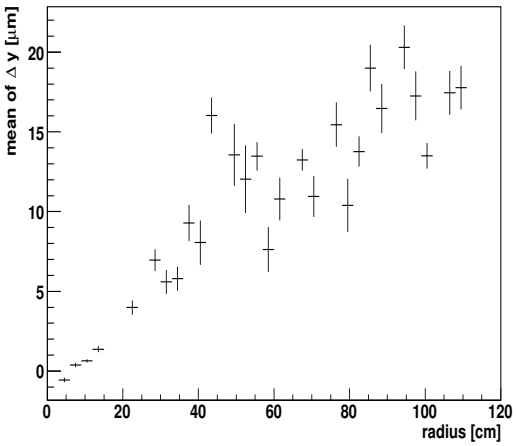

Figure 17: The r-rϕ mode 1 oscillation is visible as roughly linearly increasing mean displacement Δy as a function of the radius of the module position. The Δy of all modules are used in the plot.

4.2 Impact of Datasets

The datasets used for the alignment procedure were varied in order to study their impact. Three different dataset combinations were considered:

- Single muons from two million $Z^0 \rightarrow \mu\mu$ events;
- Single muons from 1.5 million $Z^0 \rightarrow \mu\mu$ events and half a million mass- and vertex-constrained Z^0 events;
- Single muons from two million $Z^0 \rightarrow \mu\mu$ events and 25000 high energy cosmic muons;

As an example the effects of the datasets on the shearing and bending deformations, which biases the curvature, vertex, and ϕ measurements, are presented. Figure 18 shows the average displacement of modules in the rϕ direction as a function of the module radius. As expected for bending and shearing deformations the function (equation 11) fitted through the average displacements have a nonzero slope (shearing) and curvature (bending). The results are worst when the alignment is done with single muons from the Z^0 decays only. Adding mass-constrained Z^0s only slightly improves the results. The curvature bias from the bending deformation has the opposite effect on the momentum measurements for the two differently charged muons. Hence the effect due to the reconstructed Z^0 mass is small. Adding cosmic muons to the tracks from the interaction point however, significantly improves the results. The upper and lower sections of the tracker are directly connected via the cosmic muon track. Hence the momentum and ϕ measurement in the upper and lower part must match. This is only the case if the shearing and bending deformations are small. The cosmic muons appear to be important also for the reduction of other degrees of freedom in the minimization. More details can be found in [6].

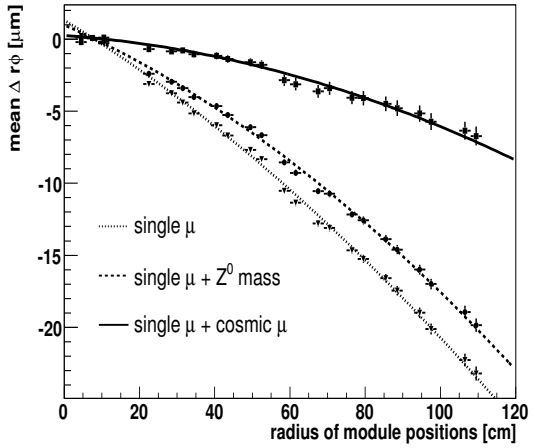

Figure 18: The mean of the displacements of barrel modules in rϕ as a function of the radius. The bending function (equation 11) is fitted to the data points.

4.3 Variation of Statistics and Event Weights

The results for the 0.5 fb^{-1} scenario are very promising, but correspond to several months of data taking. In this section how the size of the datasets affect the result is studied. Tests were also performed to understand whether happens if important datasets like the cosmic muons are given more weight in the χ^2 minimization by using the same tracks multiple times. Five different dataset combinations were tested:

- Single muons from two million Z^0 events and 5000 high energy cosmic muon events;
- Single muons from two million Z^0 $\rightarrow$ $\mu\mu$ events plus the full high energy cosmic muon dataset (25000 events);
- Single muons from one million Z^0 events and the full high energy cosmic muon dataset;
- Single muons from half a million Z^0 events and the full high energy cosmic muon dataset;

- Single muons from two million Z^0 events and using the full high energy cosmic muon dataset five times;

The results for the different datasets are summarized in table 6.
If high energy cosmics are used the result is significantly improved, as demonstrated in section 4.2. Reducing the size of the cosmic ray dataset by a factor of five has a significant impact on the results. The means on the position errors after the alignment procedure in rϕ are noticeably larger. The displacements in the other directions however, are not significantly affected by the reduced cosmic muon statistics.
If the number of single tracks from the interaction vertex is reduced by a factor of four, the precision of the module positions along the $r\phi$ coordinate is only slightly degraded. The modules measure the hit positions along the $r\phi$ direction very precisely (5-40 μm) and on average each module has thousands of hits even if only 0.5 million $Z^0 \rightarrow \mu\mu$ events are used. This means that the position would be determined to a fraction of a μm, if the global correlations of the alignment parameters were to be small. Clearly, the remaining displacements in rϕ are dominated by global deformations, and adding more tracks from the interaction point with similar energy will not improve things further. However, displacements along directions that are not so precisely measured by the module will profit more from higher statistics. The strategy of reweighting cosmic events by reusing the tracks five times only leads to slight improvements in some directions and slight degradations in others.

Table 6: The mean and RMS values for the positions of the barrel (strip and pixel) and endcap (strip and pixel) modules in $r\phi$, r and z for different dataset combinations. In the case of the Z^0 events, no mass or vertex constraints were applied.

Z^0 (single μ) [millions]	events	2	2	1	0.5	2
cosmic μ [thousands]	events	5	25	25	25	5×25
barrel $r\phi$ [μm]	mean	-7.3	-3.2	-2.2	-1.4	-2.6
	rms	9.0	8.6	8.7	9.3	8.1
barrel z [μm]	mean	-4.5	-6.9	-9.8	-11.9	-9.9
	rms	24.2	24.6	28.9	33.2	25.2
barrel r [μm]	mean	0.0	0.0	0.2	1.2	0.0
	rms	23.5	23.1	25.6	32.3	22.7
endcap $r\phi$ [μm]	mean	-9.6	-6.1	-4.9	-4.1	0.8
	rms	22.6	22.5	24.7	26.8	22.3
endcap r [μm]	mean	1.2	1.5	1.2	1.2	1.6
	rms	26.0	25.5	28.4	32.3	25.0
endcap z [μm]	mean	-10.9	13.4	-17.8	-24.5	-16.6
	rms	52.6	51.9	53.2	52.2	51.8

4.4 Impact of Outlier Rejection

To test the impact of different outlier rejection methods (section 2.6), the scenario corresponding to an integrated luminosity of 0.5 fb^{-1} (as in section 4.1) has been used.
By default the hit down-weighting method is used to treat outliers in this study. Tracks with an average hit weight below 80% are rejected. The method of rejecting tracks if the standard deviation of the track fit are large has also been tested. The cuts placed on the number of standard deviation are 54, 27, 3, 3, and 3 for the five iterations. The alignment precision achieved is similar to that reached with the default hit down-weighting method. As a further test, the number of iterations was increased from 5 to 10.
In table 7 the alignment precisions achieved are compared. The comparison clearly demonstrates that outlier rejection is essential. For example, the position uncertainty for barrel modules along the rϕ direction is reduced from 18 μm to 10 μm by the use of outlier rejection. The exact number of iterations as well as the choice of the outlier rejection method has little impact on the results.

5 Alignment Effects

The alignment results have so far been presented by comparing the true geometry parameters to the parameters found by the alignment procedure. This is clearly only possible in a simulation study, but not with real data. In the following, the physical distributions obtained from simulations with ideal geometry will be compared to the

Table 7: The mean and RMS values of the positions of the barrel (strip and pixel) and endcap (strip and pixel) modules in the $r\phi$, r and z directions. The results from different outlier rejection procedures are shown.

outlier rejection method		none	down-weighting	χ^2 cut	down-weighting
iterations		1	5	5	10
barrel $r\phi$ [μm]	mean	1.9	-1.9	1.1	-4.3
	rms	17.9	10.3	9.6	8.4
barrel z [μm]	mean	-10.9	-5.9	-7.0	-3.3
	rms	33.7	23.9	23.6	20.9
barrel r [μm]	mean	-0.8	-1.0	-0.9	-1.0
	rms	32.7	23.2	22.8	20.5
endcaps $r\phi$ [μm]	mean	-3.1	-4.7	-1.3	-6.9
	rms	31.47	23.4	23.0	19.9
endcaps r [μm]	mean	1.7	1.9	1.6	1.9
	rms	35.9	27.0	26.3	23.7
endcaps z [μm]	mean	-6.0	0.3	-0.2	2.1
	rms	44.9	42.9	42.7	40.6

corresponding distributions after alignment to illustrate the effects of the remaining misalignment.
The detector is misaligned according to the results of the alignment study using the 0.5 fb^{-1} dataset. In Figures 19 (a) and (b) the transverse momentum distributions of the reconstructed μ^+ and μ^- from the Z^0 sample are shown. In both cases no difference between the distributions with the aligned detector and with the ideal geometry can be seen. This is consistent with the fact that the bending deformation has been largely suppressed through the use of both the cosmic muons and the Z^0 mass constraint. Figure 19 (c) shows the invariant mass spectrum of the muon pairs. No significant differences between the two distributions are observed, which is to be expected, since the Z^0 mass was used as an input to the alignment procedure. The reconstructed transverse momentum of the Z^0 is also barely affected by the remaining misalignment (Figure 19 (d)). The impact on the reconstruction of the impact points (point of closest approach to the beam line) of tracks has also been studied. As was discussed in section 4.1, a small r-$r\phi$ oscillation occurred in the 0.5 fb^{-1} scenario. This was illustrated in Figure 16, which shows the average displacement in y as a function of the module radius. A straight line fit to this distribution gives the bias of the tracks arising from the residual misalignment. The point where the fit crosses the y axis, then gives the bias on the impact point position. It is found to be about -1 μm, which is consistent with what is actually observed in the impact point distributions (Figure 19(a)). The mean of the impact point distribution in the x coordinate (Figure 20 b) is 0.5 μm after alignment. This also leads to a slightly higher average impact point position in the radial direction, as can be seen in Figure 20 c. The z distribution of the impact points is very similar for both the aligned and the ideal geometry. Note that the coordinate system is defined for the purposes of this study via the average pixel barrel sensor positions. There is no reason to expect the interaction point to be exactly at the centre of the pixel detector, hence the impact point does not have to be at zero on average in real data. Only the fact that the average impact point in the simulation has been set to zero leads to the centred distribution for the ideal geometry.

Figures 19 and 20 summarize the impact of misalignment on distributions that can also be studied in real data. The effects of the misalignment are hard to detect in these rather broad distributions. The effect on the reconstructed track parameters is therefore also studied with 50000 single μ^+ tracks from a single track simulator with a transverse momentum of exactly 100 GeV. The tracks are equally distributed in ϕ and η and their vertex position is set to (0,0,0). Material interaction effects are not taken into account and a homogeneous magnetic field is assumed for the simulation of these events. The single muon events were simulated assuming the misaligned geometry, while the reconstruction assumes a perfect geometry. For all other datasets the hits are simulated with ideal geometry and the reconstruction uses a misaligned geometry, hence the alignment parameters change sign with respect to the alignment parameters discussed in previous sections.

The χ^2/ndof of the track fits is shown in Figure 21. The average χ^2 values with the ideal geometry and after the alignment are very similar. The χ^2 values with the initial misalignment are clearly much larger. The bias on the transverse momentum is illustrated in Figure 22. The initial biases are clearly almost completely removed. The reconstructed transverse momentum for all tracks is shown in Figure 23. The relative error of the transverse momentum measurement at 100 GeV increases from (1.68 $\pm$ 0.008) % to (1.72 $\pm$ 0.008) % (statistical uncertainty) if

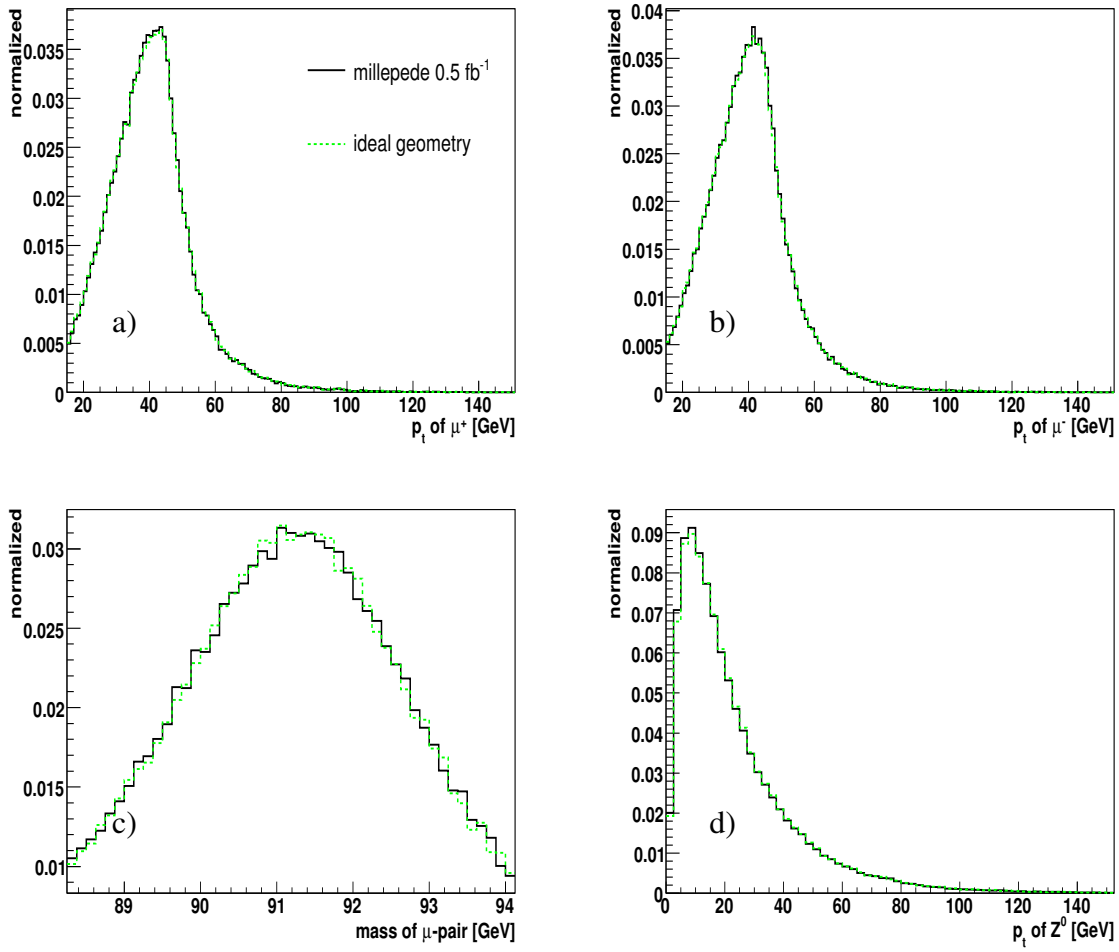

Figure 19: Comparison of different distributions for muons from the decay $Z^0 \rightarrow \mu\mu$ with ideal geometry and with the geometry determined by the alignment procedure. (a) Transverse momentum distribution for μ^+; (b) Transverse momentum distribution for μ^-; (c) Invariant mass distribution of the muon pairs and (d) transverse momentum distribution of the Z^0.

the aligned geometry is used instead of the ideal geometry. A bias in the transverse momentum of $(0.1 \pm 0.01)\%$ is introduced. The bias of the measured transverse momentum as a function of ϕ can be seen in Figure 24, for both the aligned and the ideal geometry. A very small dependence on ϕ after alignment can be seen. The impact of the remaining misalignment on the reconstruction of the point of closest approach to the beam line is shown in Figures 25 and 26. A bias of only about 1 μm of the measurement in the y coordinate is visible. The RMS of the distribution is about 7 μm with and without misalignment. Also the degradation of the measured z position of the impact point is minimal. A bias of less than 2 μm is introduced.

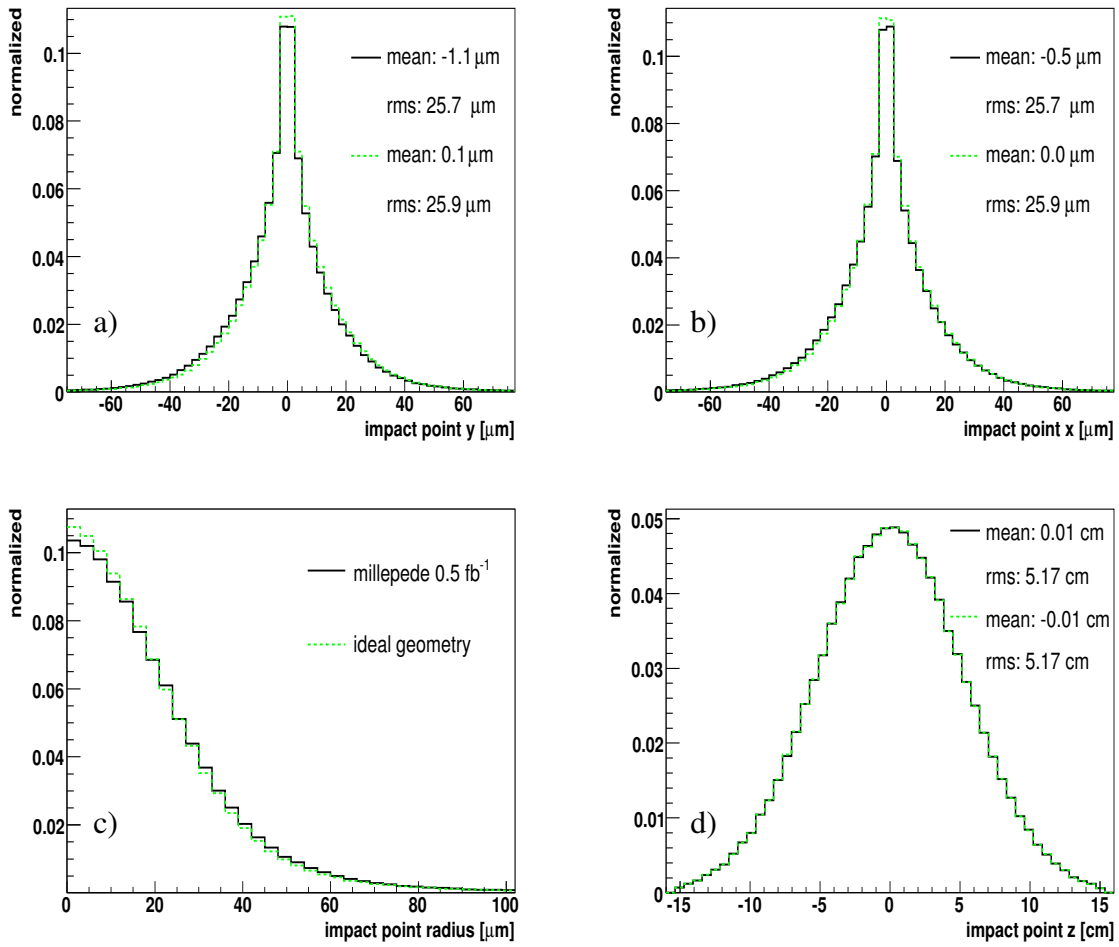

Figure 20: Comparison of resulting distributions with ideal geometry and a geometry determined by alignment using 0.5 fb^{-1} of integrated luminosity. (a) Radial position of the point of closest approach to the beam line (impact point), (b) z position of the impact point, (c) x position of the impact point, and (d) y position of the impact point.

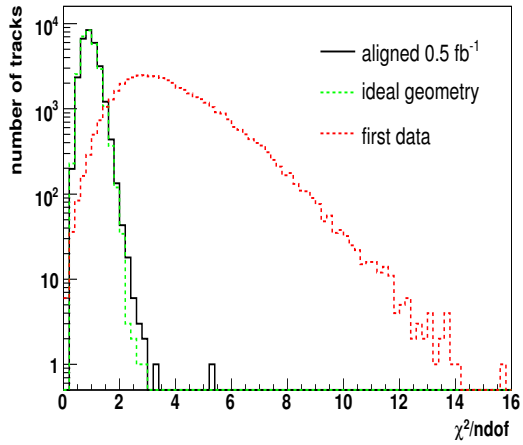

Figure 21: χ^2/ndof of track fits of 100 GeV muon tracks.

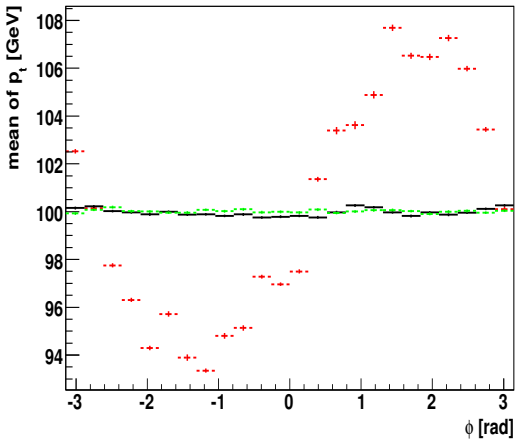

Figure 22: Mean of the reconstructed transverse momentum of 100 GeV muon tracks as a function of the azimuthal angle ϕ.

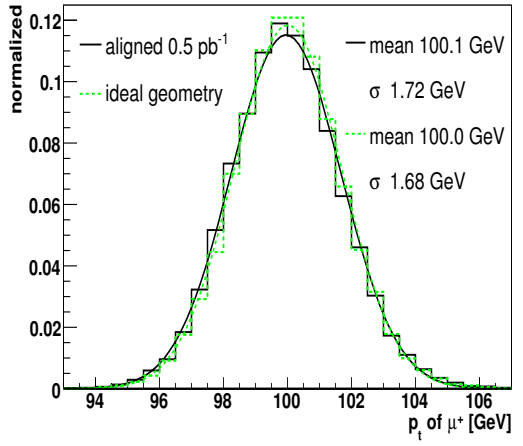

Figure 23: Reconstructed transverse momentum distributions of 100 GeV muon tracks fitted by Gaussian distribution.

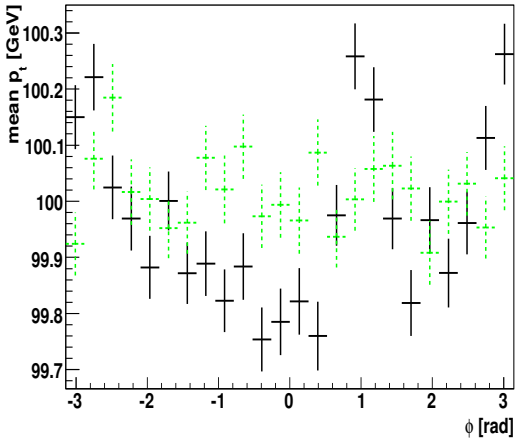

Figure 24: Average reconstructed transverse momentum of 100 GeV muon tracks as a function of ϕ.

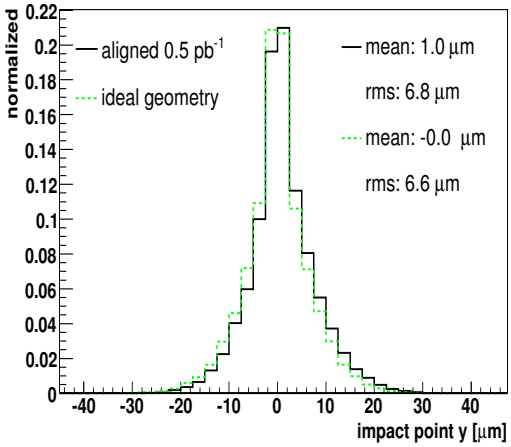

Figure 25: y-coordinate of the reconstructed impact point from 100 GeV muon tracks with a true impact point at zero.

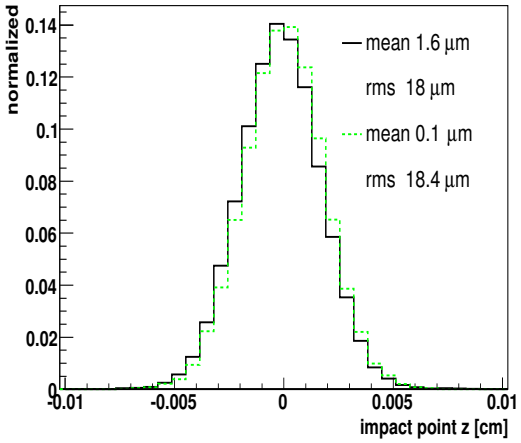

Figure 26: z-coordinate of the reconstructed impact point from 100 GeV muon tracks with a true impact point at zero.

6 Conclusions

The alignment of the CMS silicon tracking detector is a unique challenge compared to previous detectors. Sensor position uncertainties of a few μm, starting from $O(100)$ μm uncertainties, are required to fully exploit the physics potential of the tracker. In addition, the size of the tracker, with 13300 modules, is such that its alignment will be a major computational challenge, as alignment parameters for all modules need to be determined, many of which are highly correlated. The desired precision can only be achieved via track-based alignment. However, certain deformation of the tracker geometry can introduce a bias in the track parameter measurements, but leave the mean χ^2 of track fits unchanged. Given these issues, a sophisticated alignment strategy for the tracker must be developed. The alignment algorithm chosen to achieve this was Millepede II [4]. It is a non-iterative algorithm for solving χ^2 minimization problems incorporating all correlations between the geometry parameters. It is capable of dealing with the large number of position parameters (~ 50000) at CMS as well as constraints.

All possible degrees of freedom, i.e. those that can be determined by a χ^2 minimization using tracks as well as those that are χ^2 invariant, have been systematically studied. The χ^2 invariant deformations have been determined and classified. An alignment strategy is proposed which incorporates complementary sources of information which had been available as simulated data. A key ingredient in the alignment of the tracker is the use of complementary datasets like those from pp interactions at the central vertex, and cosmic ray muons, which connect different tracker parts via tracks. Vertex- and mass-constrained $Z^0 \rightarrow \mu\mu$ decays also increase the sensitivity to otherwise χ^2-invariant deformations. Position information gained during the mechanical mounting procedure and from survey measurements have also been implemented in the alignment procedure. The correlated nature of the initial displacements of the sensors (with respect to the global coordinate system) arising from the displacement of large mechanical support structures, is exploited. A hierarchical structure of alignment parameters has been introduced, which reflects the mechanical support frames.

All these ingredients were used for a full scale alignment study, aligning all modules of the CMS silicon tracker in a single procedure. A *first data* misalignment scenario, aiming to represent the displacements at startup, has been used as the starting point. Samples of events with muons from Z^0 decays and single muons corresponding to an integrated luminosity of 0.5 fb^{-1} were used, along with a sample of simulated cosmic ray muons. The module positions have been determined with an uncertainty of the order of 10 μm to 25 μm for the silicon strip sensors in the well-measured $r\phi$ direction of the sensors. For the pixel detector, a precision of a few μm was achieved. For tracks with transverse momentum of 100 GeV the bias on the transverse momentum measurement is reduced from around 7% to 0.2% at most after alignment. The transverse momentum resolution is degraded by less than 0.5% with respect to the ideal geometry. After alignment the change in the vertex position resolution is negligible and the vertex is systematically shifted by only one μm. Overall, the tracker is well aligned and the impact on physics measurements is very small. The CPU-time of the actual position parameter calculation was found to be only $\sim$2h and 2 GB of memory were required. This is remarkable, since the incorporation of all correlations is a computationally challenging task and only algorithms neglecting some or all correlations (in order to save CPU time and memory) had been proposed so far.

Studies were also performed to understand the importance of various elements of this alignment procedure. The datasets used were varied. It was found that cosmic muons are very important because they reduce a deformation (bending), which directly impacts the curvature measurement. The use of mass- and vertex-constrained Z^0 events also improved results, however they must be used in conjunction with other datasets to reduce all types of deformation to an acceptable level. This can be understood by the fact that some deformations do not strongly affect the mass measurement. A bias on the curvature measurement, for example, leads to opposite effects on transverse momentum measurement for the differently charged muons. Furthermore, the width of the Z^0 is large in comparison to the resolution. The impact of dataset size was also studied. This mimics condition before 0.5 fb^{-1} of integrated luminosity is reached. It is shown that the number of cosmic muons is very important, whilst the number of single tracks from the interaction point is less important, if the alignment precision along the well-measured $r\phi$ direction is regarded as the most relevant quantity. A further crucial issue in achieving successful alignment is the treatment of badly measured or incorrectly assigned hits. Studies showed that outlier rejection is vital. This is especially interesting, as this effect can already be observed in simulated data. Given that real data is likely to include even more outliers, it is clear that a good outlier rejection procedure must be used.

We conclude that an alignment concept for the full CMS tracker is available, which meets the requirements. However, this is a study utilizing simulated data and real data will lead to further challenges. Systematic uncertainties, like the magnetic field uncertainty or thermal movements, are not yet included. However, the alignment strategy and the developed alignment tools are fully able to take these into account once they become available. On the other hand, data from beam halo muons and laser trajectories are expected to increase the sensitivity to poorly determined deformations, hence more emphasis can be given to the event data, making the survey measurements and the support structure information less important. Unfortunately, no simulated data for beam halo muons, the laser alignment system and survey measurements had been available. Minimum bias events and decay products of low mass resonances will have to be used as well in the early phase of data taking. The alignment strategy and tools described here can be used to align the CMS tracker with real data and can be extended to use more datasets than have been discussed here.

Acknowledgment

We would like to thank Volker Blobel for many helpful discussions and for making Millepede II available.

References

[1] CMS Collaboration, *"The CMS tracker system project technical design report,"*, CERN/LHCC 98-6 CMS TDR 5, (1998).

[2] CMS Collaboration, *"Addendum to the CMS Tracker TDR by the CMS collaboration,"* CERN/LHCC 2000-16 CMS TDR Addendum 1, (2000).

[3] V. Blobel and C.Kleinwort, *"A new method for high-precision alignment of track detectors,"* Contribution to the Conference on Advanced Statistical Techniques in Particle Physics, Durham, hep-ex/0208021, March 18-22 (2002).

[4] V. Blobel, *"Millepede II manual DRAFT,"* http://www.desy.de/∼blobel (2007).

[5] V. Blobel and E. Lohrmann, *"Statistische und Numerische Methoden der Datenanalyse,"* Teubner, ISBN 3-519-03242-0, (1998).

[6] Markus Stoye, PhD thesis at the University of Hamburg, CERN-Thesis-2007-026, *"Calibration and alignment of the CMS silicon tracker"*, July (2007).

[7] R. Barrett et al. *"Templates for the solution of linear systems: building blocks for iterative methods,"* SIAM, 2nd Edition, (1994).

[8] C. C. Paige and M. A. Saunders, *"Solution of sparse indefinite systems of linear equations,"* SIAM Journal, Numerical Analysis 12, page 617-623, (1975),

[9] G. H. Golub and C. F. Van Loan,*"Matrix computations,"*(3rd ed.), Section 4.2, Johns Hopkins University Press. ISBN 0-8018-5414-8 (1996).

[10] I. Belotelov et al., *"Simulation of misalignment scenarios for CMS tracking devices,"* CMS-NOTE 2006-008, (2006).

[11] CMS Collaboration,*"Detector performance and software,"* Physics TDR Volume I, CERN/LHCC 2006-001, CMS TDR 8.1, (2006).

[12] E. Widl et al., *"Representation and estimation of trajectories from two-body decays"* CMS-NOTE 2007-032 (2007).